

# Journal of Composite Materials

<http://jcm.sagepub.com>

---

## **Time Dependent Behavior of a Particle Filled Composite PMMA/ATH at Elevated Temperatures**

Cemal Basaran, Shihua Nie and Clyde S. Hutchins  
*Journal of Composite Materials* 2008; 42; 2003  
DOI: 10.1177/0021998308094542

The online version of this article can be found at:  
<http://jcm.sagepub.com/cgi/content/abstract/42/19/2003>

---

Published by:



<http://www.sagepublications.com>

On behalf of:

[American Society for Composites](#)

**Additional services and information for *Journal of Composite Materials* can be found at:**

**Email Alerts:** <http://jcm.sagepub.com/cgi/alerts>

**Subscriptions:** <http://jcm.sagepub.com/subscriptions>

**Reprints:** <http://www.sagepub.com/journalsReprints.nav>

**Permissions:** <http://www.sagepub.co.uk/journalsPermissions.nav>

**Citations** <http://jcm.sagepub.com/cgi/content/refs/42/19/2003>

# Time Dependent Behavior of a Particle Filled Composite PMMA/ATH at Elevated Temperatures

CEMAL BASARAN\* AND SHIHUA NIE

*Department of Civil, Structural and Environmental Engineering  
State University of New York at Buffalo, Buffalo, New York, USA*

CLYDE S. HUTCHINS

*DuPont Surfaces, Yerkes R&D Laboratory, Buffalo, New York, USA*

**ABSTRACT:** Creep behavior of particle filled acrylic composite materials become a major concern when they are used at elevated temperatures. Therefore, for elevated temperature finite element simulations any constitutive modeling requires time-temperature dependent material properties. Unfortunately, this type of data is very difficult to come across in the literature, due to a very long time needed to conduct creep testing. In this study, the creep properties of acrylic casting dispersion PMMA/ATH were obtained experimentally and the observed characteristics of this material are presented with the experimental data. The underlying deformation mechanisms and the steady-state creep response are also discussed.

**KEY WORDS:** particulate composite, acrylic, creep, PMMA, ATH, viscoplasticity.

## INTRODUCTION

THE RAPID GROWTH of activities in the composites industry continues to create a need for materials that meet the difficult demands for high performance at an economical cost. When ductile matrix composite materials are reinforced by elastic inclusions of very high strength and very high modules, they lead to greater strength in shear and compression. Although reinforcements could be continuous in the form of fibers or discontinuous in the form of particles or whiskers, the particle-reinforced ductile matrix composites are widely used as they exhibit nearly isotropic properties and are often easier to manufacture. Particulate composite consists of a physical mixture of particles and a matrix, and has various choices as its particles and matrix material. In general, the addition of particles to polymer matrix can produce a number of desirable effects [1–8]. Nielsen [9] summarized the practical reasons for the use of the fillers: (a) stiffen the matrix

---

\*Author to whom correspondence should be addressed. E-mail: [cjb@buffalo.edu](mailto:cjb@buffalo.edu)  
Figures 2, 5–18 and 21–24 appear in color online: <http://jcm.sagepub.com>

and make it more rigid; (b) regulate the coefficient of thermal expansion and thermal shrinkage of the matrix material; (c) improve heat resistance; (d) reduce creep; (e) increase the strength properties of the polymer matrix material; (f) modify the permeability behavior to gases and liquids; (g) improve electrical properties; (h) modify rheological properties; and (i) lower the cost of the material.

The acrylic casting dispersion PMMA/ATH stands for lightly cross-linked polymethylmethacrylate (PMMA) filled with about by a fine dispersion of alumina trihydrate (ATH). In this composite material the average size of ATH filler particles is 2–10  $\mu\text{m}$ , which occur as agglomerates of 3  $\mu\text{m}$  (average) and volume fraction of the ATH is 48%. The 7 mm thick sheets are manufactured by continuous casting process with slow cooling to minimize warping and residual stresses [10].

PMMA/ATH is used as a substitute for many indoor ceramic applications. Because of its lower cost, the ease of molding, and wear resistance (largely due to reinforcement particles of ATH), this composite material is preferred to natural marbles. Some examples are counter-tops, kitchen sinks and bathroom vanities. PMMA is an amorphous glass below 110°C and exhibits ductile fracture under normal conditions at room temperature. PMMA, because of its molecular chains viscoelastic/plastic properties, is very sensitive to strain rate and temperature. Creep phenomenon is particularly common in polymers. For polymers, the delayed response of polymer chains during deformations is the cause of creep behavior. Deformation stops when the initially folded chains reach a new equilibrium configuration. Part of this stretching of chains is recoverable after load is removed, but recovery takes place slowly with the chains retracting by folding back to their initial state. It is a well known observation that as the temperature decreases, or loading rate increases, both yield stress and Young's modulus increase [11]. Since PMMA/ATH acrylic casting dispersion is being used increasingly for thermal load-bearing applications, understanding the creep process is essential if they are to be used in a safe and reliable fashion.

Presented in this study are the results of a series of experimental studies conducted at various temperatures and loading rates. This study was conducted because of a lack of such published data in the literature which is needed for constitutive modeling [12].

## EXPERIMENTAL PROCEDURE

Composite material properties are sensitive to the manufacturing process. Specimens manufactured in the laboratory have different properties than industrial manufacturing line samples. Therefore, for this study specimens were cut from a sheet of 7 mm thick plate that was manufactured on an industrial production line (shown in Figure 1). The uniaxial tension, uniaxial compression and creep tests were performed in a servo-hydraulic MTS material characterization unit, type 858 Table Top System (10 kN capacity), controlled by a personal computer and fitted with an ATS 7510 thermal chamber for the control of ambient temperature. The test system has load, stroke, and strain control capacity. The accuracy of temperature control is about 1°C and is monitored by using an ATS feedback control system and a thermocouple. Time-dependent testing requires hydraulic grips. The test system also includes an interchangeable 685.22 side-loading hydraulic wedge grip system with grip pressure up to 3000 psi. The hydraulically-actuated grip system is independently activated and could maintain an adjustable grip force on the specimen grip face without a backlash. Grips are attached to the load frame via a fixed, but adjustable, alignment system. The MTS 634.25 axial extensometer (from +50 to –10%), with a gauge

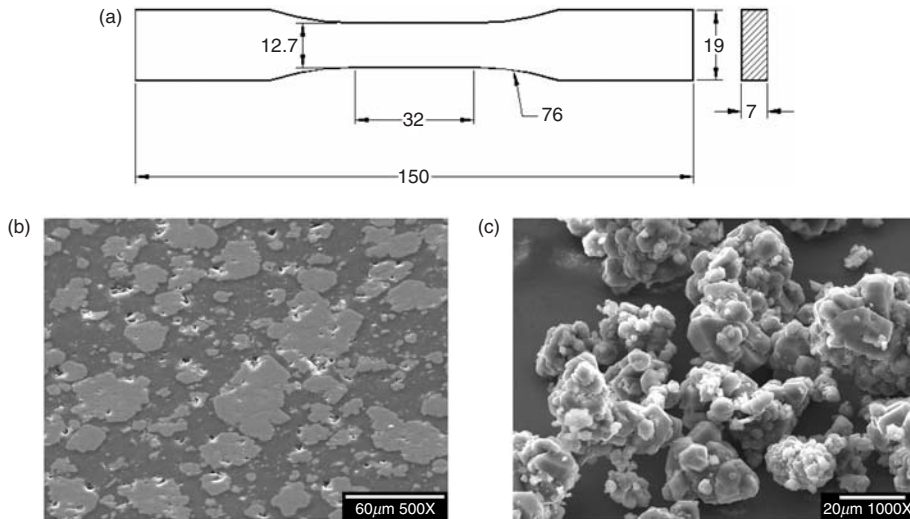


**Figure 1.** (a) Specimen geometries (mm), (b) polished surface of Sample (gray regions are particles), (c) ATH Filler Particles Under SEM.

length of 2 inches, is used to measure uniaxial strain in the testing. The experiments were conducted as a function of strain rate and temperature for uniaxial tensile and compressive tests. The strain rate ranged over three decades from  $1 \times 10^{-3}$  to  $1 \times 10^{-7} \text{ s}^{-1}$ , and temperatures varied from room temperature to  $90^\circ\text{C}$ . Because of space limitations not all data obtained in this study is presented here, albeit a representative of the overall behavior. For complete data, readers are referred to Nie [13]. The details of the procedures used in this work are described in ASTM D 638-98 [14].

The initial loading rate has an impact on the creep response observed. Thus it is necessary to specify and control both the creep stress and initial loading rates in creep experiments. In this work, the load rate of 0.5 kN/s is used for all experiments. At  $T=22^\circ\text{C}$ , the ultimate tensile load for the test specimen is about 4.0 kN. Creep tests were performed under a constant force of 3.6 kN (90% of ultimate tensile load), 3.2 kN (80%), and 2.4 kN (60%) in tension. Creep tests were also performed under the force of 3.2 kN (80% of ultimate tensile load) in compression. At  $T=75^\circ\text{C}$ , the ultimate tensile load for the test specimen is 2.5 kN. Creep tests under 2.2 kN (88% of ultimate tensile load); 2.0 kN (80%), 1.5 kN (60%), 1.0 kN (40%), 0.5 kN (20%), and 0.25 kN (10%) were performed in tension. Creep tests under 2.2 kN (88% of ultimate tensile load) were also performed in compression. (Ultimate compressive strength of this composite material could not be obtained because of testing system limitations, and unfortunately it is not available in the literature, to the best of our knowledge.)

## RESULTS AND DISCUSSION

### Uniaxial Tensile and Compressive Tests

The uniaxial extension experiment results for different temperatures is shown in Figure 2, indicating that, as expected, temperature has a significant influence on the

mechanical behavior of this composite material, in spite of the fact that the filler particles' melting temperature is about 3500°C. At room temperature (22°C) PMMA/ATH is brittle and fails under tension long before a major elongation or any plastic strain is achieved, (Figure 2). At temperatures over 75°C, PMMA/ATH behaves like as a ductile material: first it reaches the peak load, and then the load capacity decreases with the increasing of strain until failure. This observed behavior indicates that viscoplasticity must be considered at high temperature finite element simulations.

Typical stress–strain curves obtained for different strain rates under uniaxial tensile tests on PMMA/ATH at room temperature are shown in Figure 3. An important effect of the strain rate on these stress–strain curves is observed. The material stiffness and ultimate stress increased as the strain rate increased. The stress–strain curve is initially linear elastic to a critical stress level (about 25 MPa) then it starts to behave non-linearly. After the onset of continuous non-linear behavior, the stress–strain curve reaches the peak point and the failure of the specimen occurs suddenly before a significant plastic strain is achieved [13]. The initial elastic region of the curve is controlled primarily by the inclusion concentration.

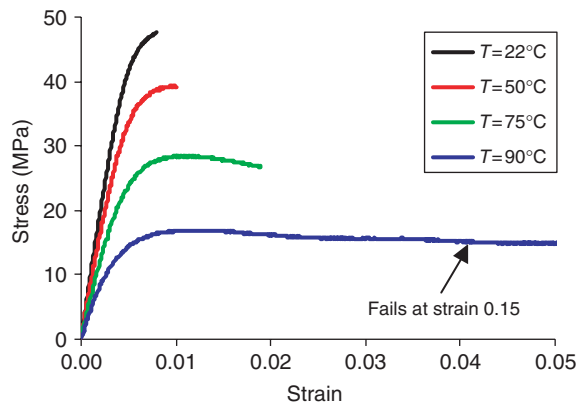


Figure 2. Uniaxial stress–strain curves of PMMA/ATH at different temperatures with strain rate of  $1 \times 10^{-4} \text{ s}^{-1}$ .

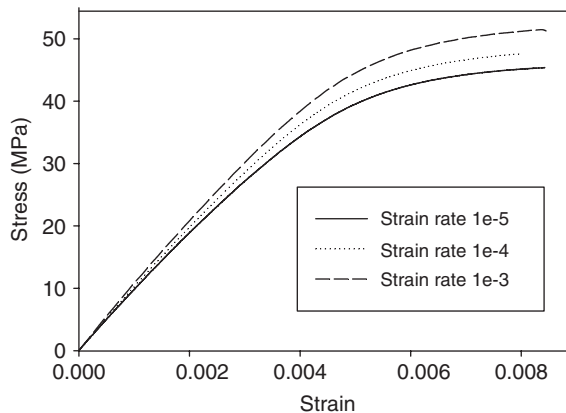


Figure 3. Uniaxial tension stress–strain behavior of at different strain rates and 22°C.

Elastic modulus of ATH is 70 GPa compared to PMMA matrix elastic modulus of 3.5 GPa. Application of strain in the last region of the curve is only to stretch the binder and enlarge existing cavities.

Monotonic stress–strain curves obtained from the compressive tests are shown in Figure 4 for several different strain rates. It is shown clearly that the composite material exhibits markedly different behavior in compression than in tension. This is due to the microstructure of particle-reinforced ductile matrix composites. In tension, the particles act as stress concentrators, while in compression the particles serve to transmit stresses. The resulting material is brittle in tension, but in compression it is similar in behavior to ductile matrix at room temperature. The compressive test was terminated at 0.008 strain due to maximum load carrying capacity of the load cell used in the system.

### Creep Tests

Creep, time-dependent deformation, is generally viewed as a stress driven process that is significantly influenced by temperature. In polymer matrix composites, creep is controlled by stretching of molecular chains rather than the diffusion process that dominates creep in poly-crystalline materials. ATH is a poly-crystal structured material with a very high melting temperature, about 3500°C. Therefore time-dependent behavior is mainly controlled by PMMA, which has a very low glass transition temperature of about 110°C. In standard uniaxial creep tests, the load is constant and the creep stress is defined as the applied load divided by the initial test specimen area. Mathematically and experimentally, the creep strain is defined as the difference between the total measured strain and the calculated elastic strain. The most common representation of the creep data is a plot of creep strain as a function of time, where each curve represents the creep strain response for constant values of temperature and stress. The variation of creep strain as a function of time for different stresses is given in Figures 5 and 6 at temperatures of 75 and 22°C, respectively. The variation of creep strain rate as a function of time with different stresses is given in Figures 7 and 8 at temperatures of 75 and 22°C, respectively. Here the creep strain and creep strain rate are measured in terms of micro strain and micro strain per second, respectively.

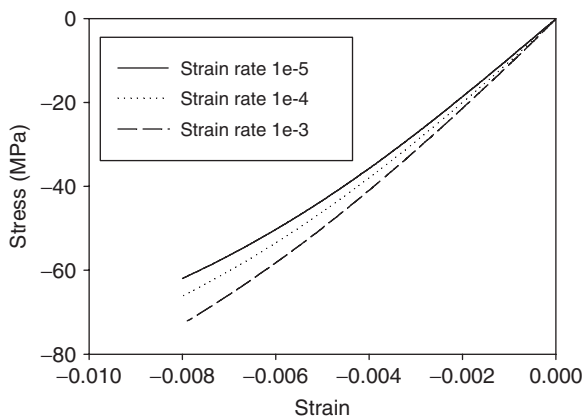


**Figure 4.** Uniaxial compressive stress–strain behavior at different strain rates at 24°C.

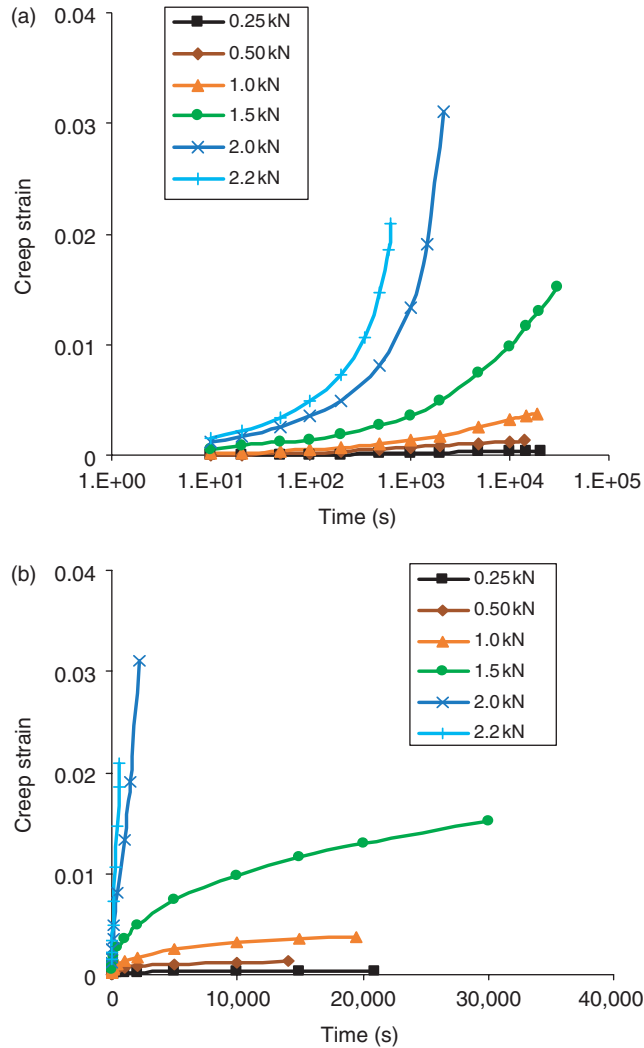


**Figure 5.** Time dependent strain response at 75°C for different values of load as plotted on (a) logarithmic scale, (b) linear scale.

As shown in Figures 5–8, the initial creep strain rate (primary creep) can be relatively high. Then the primary creep strain rate decreases to a steady-state rate. Eventually, the creep rate increases from the steady-state value and unrestrained flow occurs (tertiary creep) leading to rupture. As expected, the primary, secondary, and tertiary creep rates and the time to rupture were strong functions of the creep stress and temperature. Increasing the stress and temperature increased the creep rate and reduced the time to rupture. In Figure 7, we observe that at 75°C for load 2 kN and higher tertiary creep is reached very quickly.

The creep strength and rupture strength are frequently reported material properties. Creep strength is defined as the stress that produces the steady-state creep rate at a specified temperature. For example for the creep rate of  $1 \times 10^{-6} \text{ s}^{-1}$ , the creep strength

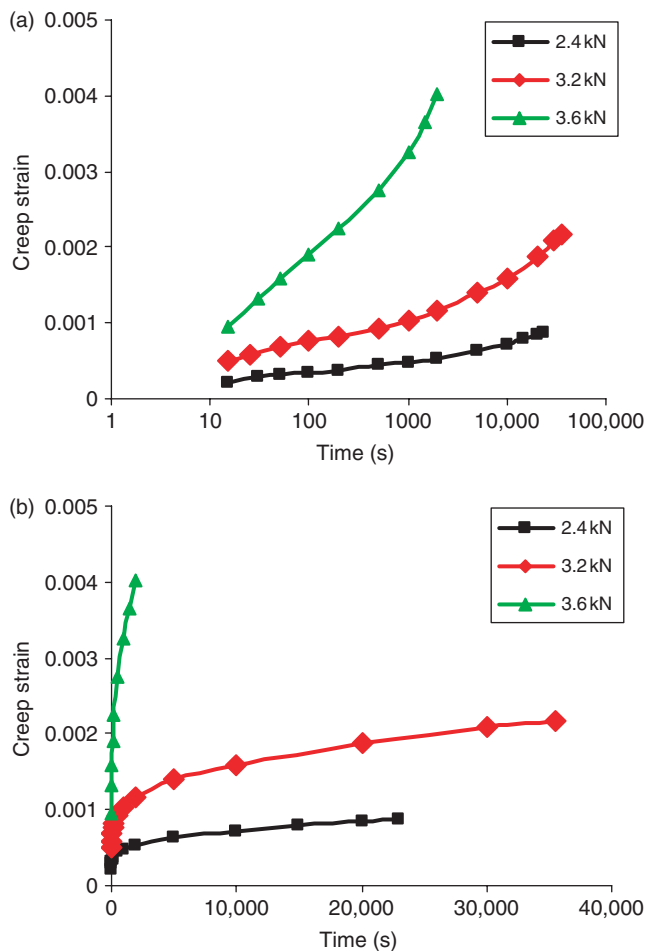


Figure 6. Time dependent strain response of PMMA/ATH at 22°C for different values of load as plotted on (a) logarithmic scale, (b) linear scale.

of PMMA/ATH at 75°C is about 19 MPa as shown in Figure 9. The creep strength can also be defined as the stress to produce a specified creep strain for a specified time and temperature.

The increase in primary creep strain as a function of temperature at the stress level of 25 MPa is shown in Figure 10.

Plots for the creep strain rate and creep strain in both tension and compression at 22°C are shown in Figures 11 and 12, respectively. Although the creep strain in tension is greater than that in compression, Creep strain rate is almost the same in tension and compression at  $T=22^{\circ}\text{C}$ . Moreover, the steady-state creep strain rate at 22°C is very small, so PMMA/ATH can be regarded as rate-insensitive materials at room temperature.

Creep behavior is very different in tension and in compression at  $T=75^{\circ}\text{C}$ , as shown in Figures 13 and 14. The results show that for nearly the same magnitude of stress in tension and compression, the magnitude of the creep rates in tension is much greater than that in compression. This difference is due partly to the fact that that the creep tests

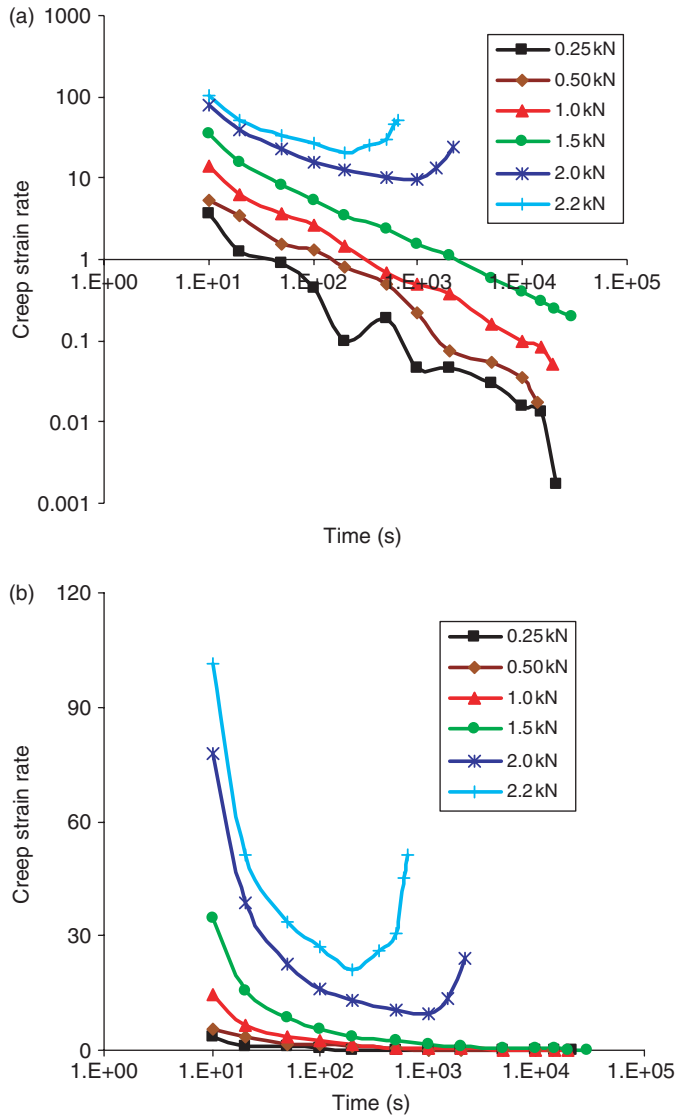


**Figure 7.** Time dependent strain rate response at 75°C for different values of load (a) logarithmic scale, (b) linear scale.

are constant-load, not constant-stress tests. The creep stress is defined as the constant load divided by the initial specimen area. Therefore, in a tensile test the true stress increases as the specimen area decreases, and in compression the true stress decreases as the specimen area increases as a result of Poisson ratio effects. We believe the most important reason for different response in tension and compression is the de-tanglement of molecule chains, which is the dominant time-dependent deformation mechanism in PMMA matrix. Tensile stresses expand the chains and reduce the resistance to de-tanglement, whereas compressive stresses reduce the chain dimensions and increase the resistance for de-tanglement.

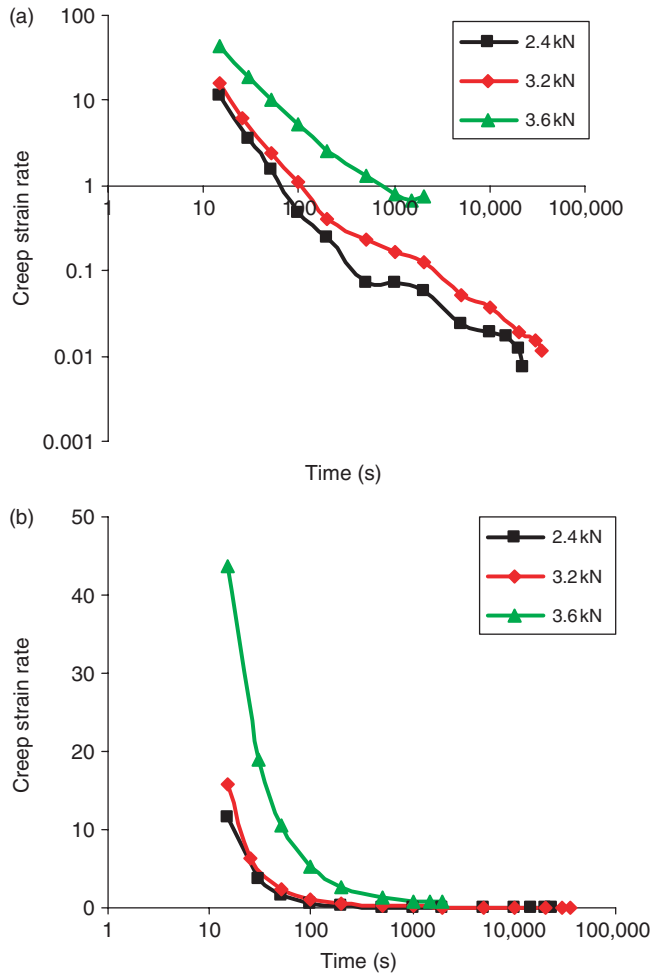


**Figure 8.** Steady-state creep strain rate as a function of time at 22°C for different values of load (a) logarithmic scale, (b) linear scale.

### Constitutive Modeling

A micro-mechanics based constitutive model for particle filled composites has been developed and published by Nie and Basaran [14] and Basaran and Nie [12]. In here we summarize the main points of the model. The model characterizes the composite as a three different constituents, matrix, filler particle and inter-phase (bonding agent between filler and particle) (Figure 15). However, in the formulation filler particle and inter-phase are homogenized to a single phase.

### Viscoplastic Behavior of Two-phase Composites

Assuming a perfectly bonded two-phase composite consisting of a viscoplastic matrix (phase 0) with an elastic bulk modulus  $k_0$  and elastic shear modulus  $\mu_0$ , and randomly

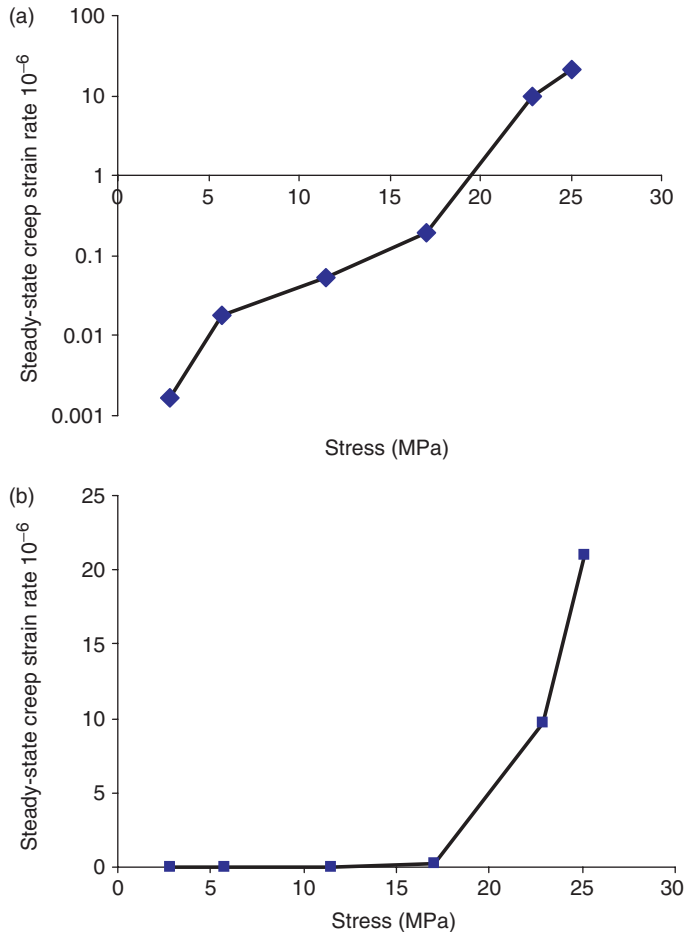


**Figure 9.** Effects of stress on the nominal stationary creep strain rate of PMMA/ATH at 75°C as plotted on (a) logarithmic scale, (b) linear scale.

dispersed elastic spherical particle–interphase assembly (Phase 1) with effective bulk modulus  $k_1$  and effective shear modulus  $\mu_1$ . The effective elastic moduli of the two-phase composite by neglecting the inter-particle interaction effects can be given as Ju and Chen (1994a):

$$k = k_0 \left\{ 1 + \frac{3(1 - \nu_0)(k_1 - k_0)\phi}{3(1 - \nu_0)k_0 + (1 - \phi)(1 + \nu_0)(k_1 - k_0)} \right\} \tag{1}$$

$$\mu = \mu_0 \left\{ 1 + \frac{15(1 - \nu_0)(\mu_1 - \mu_0)\phi}{15(1 - \nu_0)\mu_0 + (1 - \phi)(8 - 10\nu_0)(\mu_1 - \mu_0)} \right\} \tag{2}$$

where  $\phi$  is the particle volume fraction and,  $\nu_0$  is Poisson’s ratio of the matrix.

In the model it is assumed that viscoplastic yielding and flow occur only in the matrix, and the matrix solely determines the viscoplastic behavior of the composite. The latter assumption is based on the fact that glass transition temperature for PMMA is

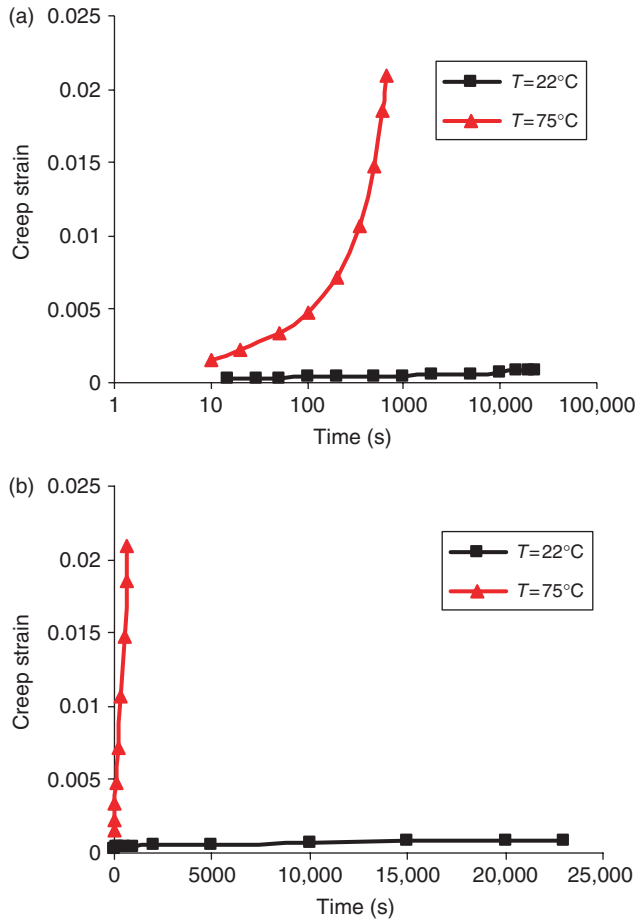
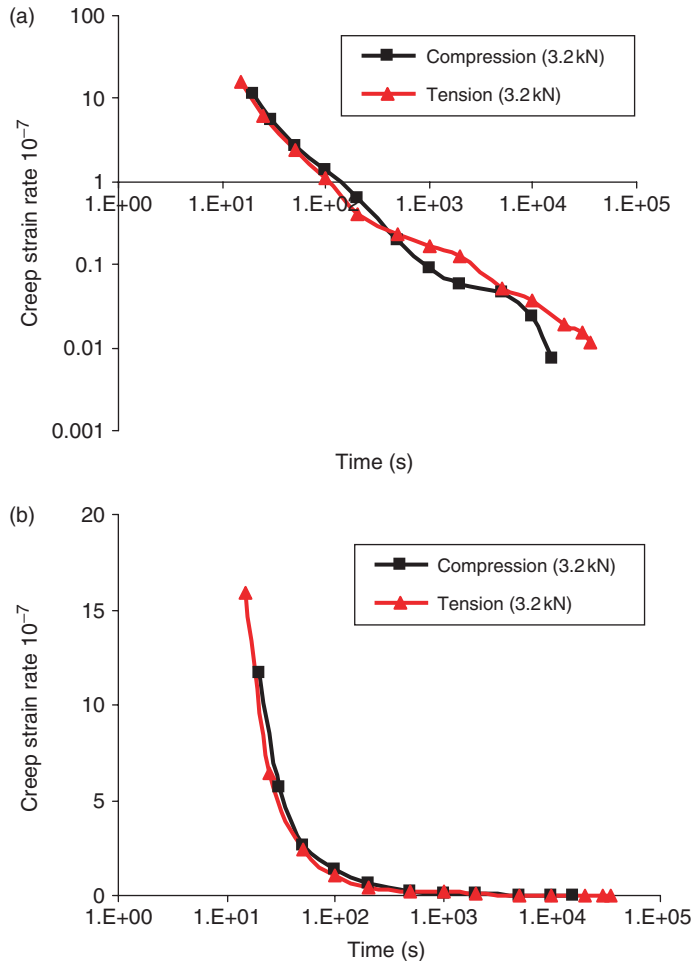


Figure 10. Creep strain as a function of time at 25 MPa for different temperatures (a) logarithmic scale, (b) linear scale.

around 110°C, however, for ATH the melting temperature is around 3500°C. Based on these temperatures, the latter assumption is, we believe, valid. The magnitude of the current equivalent stress norm of the matrix can be utilized to determine the possible viscoplastic behavior in the composite. When the ensemble-volume averaged current stress norm in the matrix reaches a certain level, the composite undergoes viscoplastic flow. The effective yield function for the composite in the presence of CTE mismatch induced stresses can be written as:

$$f(\bar{\sigma}, \bar{\alpha}) = \sqrt{(\bar{\sigma} - \bar{\sigma}^T) : \bar{\mathbf{T}} : (\bar{\sigma} - \bar{\sigma}^T)} - \sqrt{\bar{T}_1 + 2\bar{T}_2 \bar{\sigma}_Y(\bar{\alpha})} \quad (3)$$

where  $\bar{\sigma}$  is the average stress in the composite,  $\bar{\sigma}^T$  is the stress caused by CTE mismatch between the ATH filler and the PMMA matrix,  $\bar{\mathbf{T}}$  is a fourth order tensor,  $T_1$  and  $T_2$  are factors given in Basaran and Nie [12], that account for influence of particles on the matrix



**Figure 11.** Creep strain rate in tension and compression at 22°C as a function of time (a) logarithmic scale, (b) linear scale.

yield stress,  $\bar{\sigma}_y(\bar{\alpha})$  is the isotropic hardening function of the composite materials,  $\bar{\alpha}$  is the equivalent viscoplastic strain that defines isotropic hardening of the yield surface of the composites, and:

$$\dot{\bar{\alpha}} = \sqrt{\bar{T}_1 + 2\bar{T}_2} \sqrt{\dot{\bar{\epsilon}}^{vp} : \bar{\mathbf{T}}^{-1} : \dot{\bar{\epsilon}}^{vp}}. \tag{4}$$

The factors in the effective yield and effective plastic strain increment equations are chosen so that the effective stress and effective plastic strain increments are equal to the uniaxial stress and uniaxial plastic strain increment in a tensile test. It should be noted that the effective yield function is pressure dependent now (as a result of accounting for CTE mismatch) and no longer of the Von-Mises type. Therefore, the particles have significant effect on the viscoplastic behavior of the matrix.

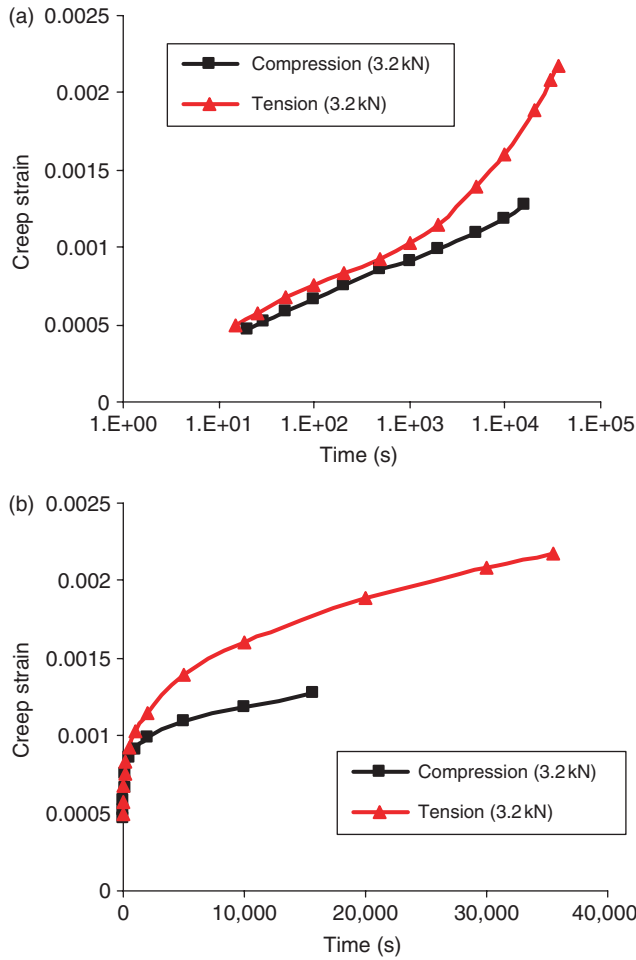


Figure 12. Creep strain in tension and compression for PMMA/ATH at 22°C as plotted on (a) logarithmic scale, (b) linear scale.

In order to simulate damage evolution behavior of composite materials, there is a need for introduction of a damage parameter in the above proposed constitutive model. Damage mechanics provide us with basic framework to develop damage evolution models. According to the strain equivalence principle, the effective damage coupled yield function for an isotropic damage parameter  $D$  can be written as:

$$f(\bar{\sigma}, \bar{\alpha}) = \sqrt{\left(\frac{\bar{\sigma}}{1-D} - \bar{\sigma}^T\right) : \bar{T} : \left(\frac{\bar{\sigma}}{1-D} - \bar{\sigma}^T\right)} - \sqrt{\bar{T}_1 + 2\bar{T}_2 \bar{\sigma}_y(\bar{\alpha})} \quad (5)$$

where  $D$  is the damage parameter. It is obvious that the damage increases the equivalent stress norm of the composite, which tends to amplify the viscoplastic flow of the composite.

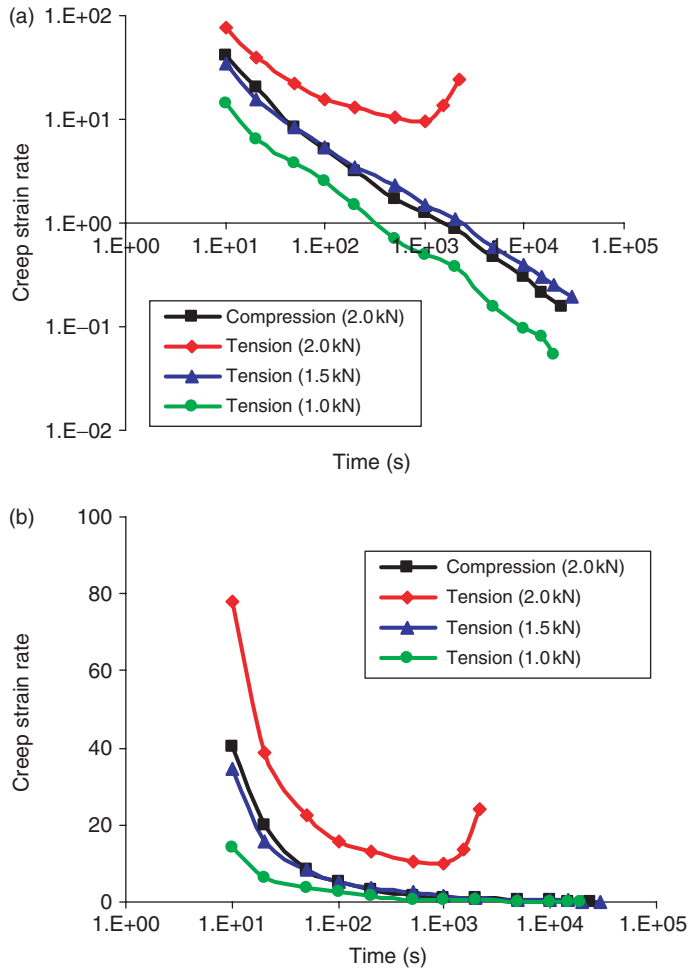


Figure 13. Creep strain rate in tension and compression at 75°C (a) logarithmic scale, (b) linear scale.

A perzyna-type viscoplasticity flow model is employed to characterize the rate dependency (viscosity) behavior of the matrix. It is assumed that viscoplastic flow that takes place in the matrix follows the Perzyna model, where creep strain rate is proportional to over-stress and viscosity coefficient of the material. Therefore, the effective ensemble-volume averaged plastic strain rate for the composite can be expressed as:

$$\dot{\epsilon}^{vp} = \gamma \frac{\partial f}{\partial \boldsymbol{\sigma}} = \frac{1}{1 - D} \gamma \mathbf{n} \tag{6}$$

where  $\dot{\epsilon}^{vp}$  is the creep strain rate:

$$\mathbf{n} = \frac{\bar{\mathbf{T}}((\bar{\boldsymbol{\sigma}}/1 - D) - \bar{\boldsymbol{\sigma}}^T)}{\sqrt{((\bar{\boldsymbol{\sigma}}/1 - D) - \bar{\boldsymbol{\sigma}}^T) : \bar{\mathbf{T}} : ((\bar{\boldsymbol{\sigma}}/1 - D) - \bar{\boldsymbol{\sigma}}^T)}} \tag{7}$$

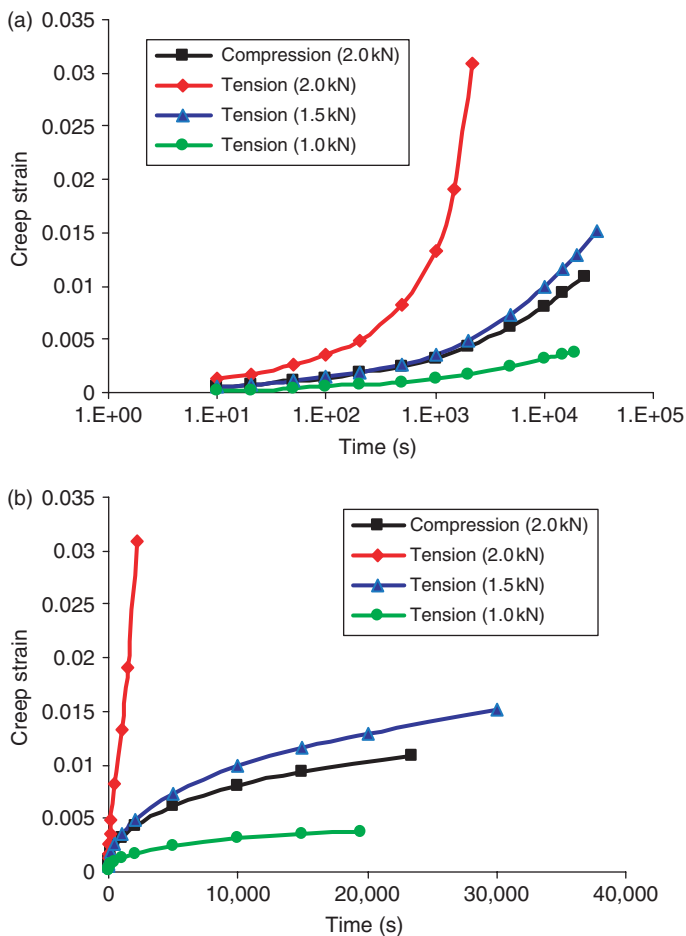


Figure 14. Creep strain in tension and compression at 75°C (a) logarithmic scale, (b) linear scale.

and  $\gamma$  denotes the plastic consistency parameter given by

$$\gamma = \frac{\langle f \rangle}{\eta} = \frac{\langle f \rangle}{2\mu\tau} \tag{8}$$

$\eta$  is viscosity coefficient,  $\tau$  is relaxation time, and the equivalent plastic strain is defined as:

$$\dot{\alpha} = \sqrt{\bar{T}_1 + 2\bar{T}_2} \frac{\gamma}{1-D} \tag{9}$$

### Determination of Material Parameters from Test Data

In order to successfully simulate the damage coupled viscoplasticity of particulate composites, it is important to determine the appropriate material parameters for the model. Experimental tests that simulate in-service loading conditions are required to

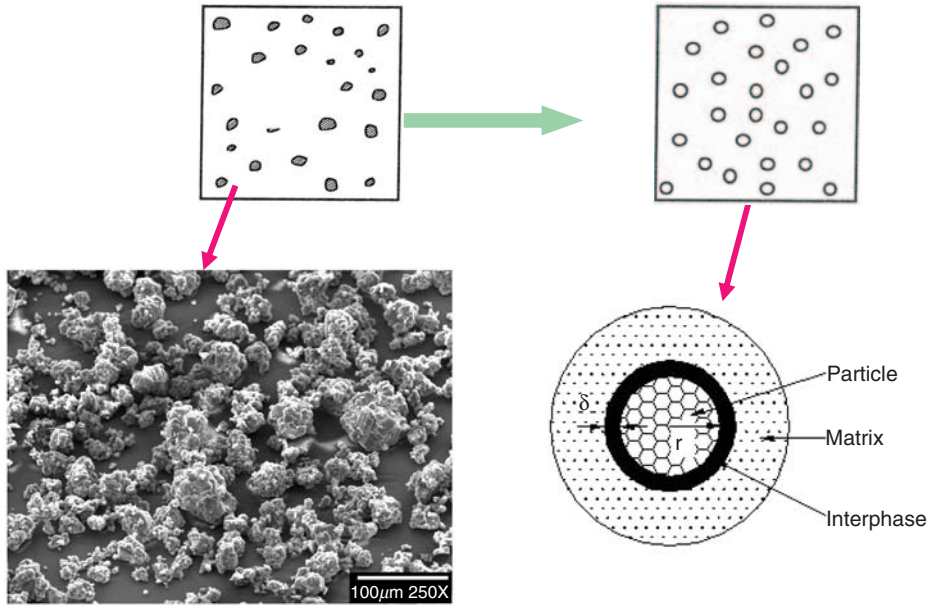


**Figure 15.** Three-phase composite system.

obtain reliable material parameters needed by the constitutive model. Due to the time and temperature dependent mechanical properties of acrylic particulate composites, it is desirable that tests are conducted under different loading rates and different temperatures.

The material parameters needed for the constitutive model can be obtained from the test data presented in the previous section.

### Viscosity Coefficient

Material properties for viscoplastic flow function can be obtained from strain rate vs. stress plots. In Equation (6) there are four terms: viscoplastic strain rate, yield function, stress, and plastic strain consistency parameter  $\gamma$ . The strain rate, yield function, and stress value are known (see Figure 9(a)). We can calculate the  $\gamma$  value for each point in the strain rate vs. stress curve, and fit an empirical curve to experimental data to obtain  $\eta$ .

### Properties of ATH

In the model, ATH is regarded as an isotropic elastic material. The thermomechanical properties of ATH as provided by the manufacturer are as follows:

Poisson ratio of ATH:  $\nu_f = 0.24$

Elastic modulus of ATH:  $E_f = 70000 \text{ MPa}$

Coefficient of thermal expansion of ATH:  $\alpha_f = 1.47 \times 10^{-6} / ^\circ\text{C}$

The average diameter of ATH is  $35 \mu\text{m}$ .

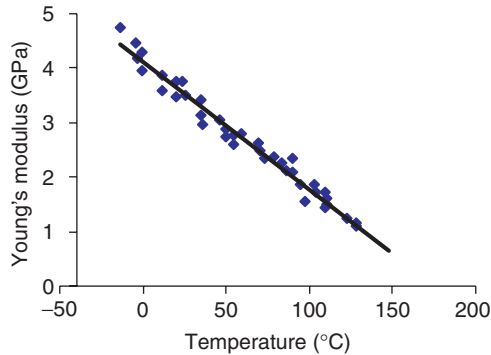


**Figure 16.** Young's modulus of PMMA as a function of temperature [1–3].

### Properties of PMMA

The matrix PMMA is a very common polymer, which has been extensively studied. Young's modulus of PMMA as a function of temperature is taken from the works of Cheng et al. [1–3] as shown in Figure 16:

$$E_m = -0.0234T + 4.124(\text{GPa})$$

where  $T$  is the temperature in Celsius.

Poisson's ratio of PMMA provided by the manufacturer was  $\nu_m = 0.31$ . The CTE of PMMA is assumed to be the same as that of the particulate composite.

### Properties of Interphase

The interphase around the particle is also regarded as an isotropic elastic material. Young's modulus and thickness of the interphase are adjustable parameters in the proposed model. In addition, it is reasonable to assume that the Poisson ratio and CTE of the interphase are the same as that of the matrix (PMMA), however, Young's modulus of the interphase is less than that of PMMA.

### Properties of Particulate Composites

The following thermomechanical properties of the particulate composite  $A$  are determined according to the data provided by the manufacturer.

The average specific mass for the composite:  $m_s = 85 \text{ g/mole}$

Density of the composite:  $\rho = 1750 \text{ Kg/m}^3$

Volume fraction of particle in the composite:  $\phi = 0.48$ .

Poisson's ratio of the composite  $A$  is given as a function of temperature as shown in Figure 17:

$$\nu = 0.008T + 0.334.$$

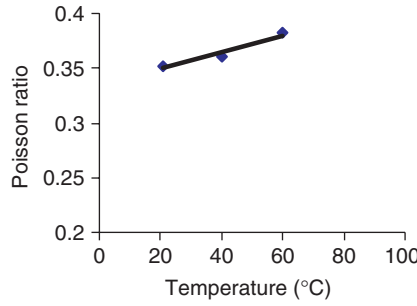


**Figure 17.** Poisson's ratio of composite A as a function of temperature.

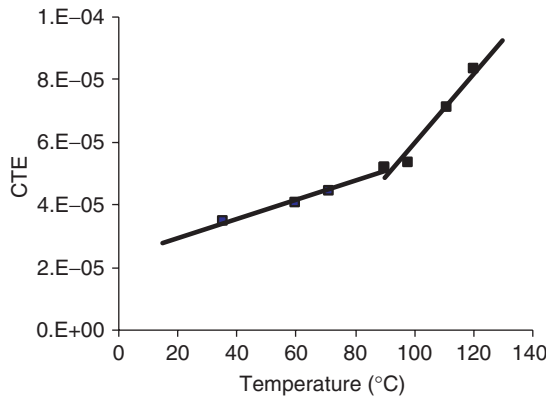


**Figure 18.** Coefficient of thermal expansion (CTE) of composite A as a function of temperature.

The coefficient of thermal expansion of the composite A is given as function of temperature as shown in Figure 18. When  $T \leq 90^\circ\text{C}$ :

$$\alpha = 3.035 \times 10^{-7}T + 2.347 \times 10^{-5}. \tag{10}$$

When  $T \geq 90^\circ\text{C}$

$$\alpha = 1.0992 \times 10^{-6}T - 5.012 \times 10^{-5}. \tag{11}$$

The viscosity relaxation time  $\tau$  is defined as (Simo and Hughes, 1998)

$$\tau = \frac{\eta}{2\mu}$$

where  $\mu$  is the shear modulus and  $\eta$  is the viscosity. The viscosity relaxation time  $\tau$  is determined as shown in Figure 19. When  $T \leq 90^\circ\text{C}$

$$\tau = 1.12406 \times 10^{-6}T^3 - 1.67823 \times 10^{-4}T^2 + 7.91134 \times 10^{-3}T + 7.35 \times 10^{-3}. \tag{12}$$

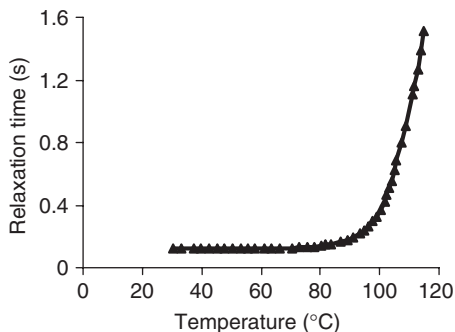


Figure 19. Relaxation time of composite A as a function of temperature.

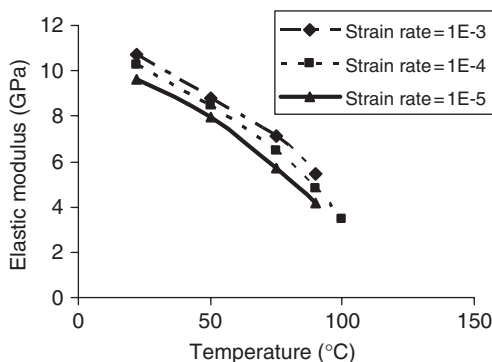


Figure 20. Elastic modulus of composite A as a function of temperature.

When  $T \geq 90^\circ\text{C}$ :

$$\tau = -2.6348 \times 10^{-6} T^4 + 1.08452 \times 10^{-3} T^3 - 1.64629 \times 10^{-1} T^2 + 10.9673 T - 271.11. \quad (13)$$

The elastic modulus of composite *A* can be determined from the properties of the particle, the matrix and the interphase according to the proposed micromechanical model for particulate composites. The elastic modulus of composite is also determined from our uniaxial tensile tests with a different strain rate and temperature as shown in Figure 20:

$$E_m = -0.0005 T^2 - 0.021 T + 13.33 + 0.6 \log(\dot{\epsilon}) \text{ (GPa)}. \quad (14)$$

The gas constant is also needed for the damage evolution function, where its value is given as follows:  $R = 8.3145 \text{ J/mole/K}$ .

### Isotropic Hardening Parameters

The Ramberg–Osgood isotropic hardening model is used to model the monotonic tensile yield stress, which is reasonably accurate for the uniaxial tensile behavior.

$$\bar{\sigma}_y = \bar{\sigma}_0 + K \bar{\alpha}^n$$

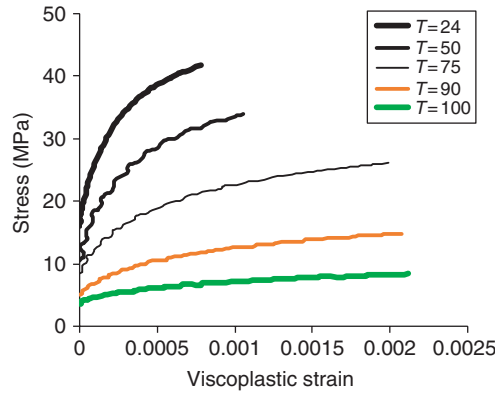


Figure 21. Stress as a function of viscoplastic strain for composite A at various temperatures.

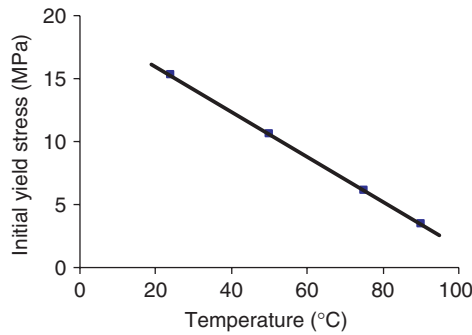


Figure 22. Initial yield stress of composite A as a function of temperature.

where  $\bar{\sigma}_0$  is the initial yield of stress for composite A and  $\bar{\alpha}$  is the equivalent viscoplasticity,

$$\dot{\bar{\alpha}} = \sqrt{\bar{T}_1 + 2\bar{T}_2} \sqrt{\dot{\bar{\epsilon}}^{vp} : \bar{\mathbf{T}}^{-1} : \dot{\bar{\epsilon}}^{vp}}$$

The temperature dependent constants  $K$  and  $n$  for the Ramberg–Osgood isotropic hardening model can be easily determined from experimental data near the yield point, where the damage is believed to be negligible. Experimental data for the stress as a function of the viscoplastic strain for the composite at various temperatures is shown in Figure 21.

The parameters for the Ramberg–Osgood isotropic hardening model are determined from the monotonic uniaxial tensile tests at various temperatures, Figure 21. The results are shown in Figures 22–24.

$$\bar{\sigma}_0 = -0.1791T + 19.6, \quad T \leq 100^\circ\text{C}$$

$$K = -8.5881 \times 10^{-4}T^3 + 9.1312 \times 10^{-2}T^2 - 4.8155T + 424.9, \quad T \leq 100^\circ\text{C}$$

$$n = 4.098 \times 10^{-7}T^3 - 4.476 \times 10^{-5}T^2 + 2.33 \times 10^{-3}T + 0.3542, \quad T \leq 100^\circ\text{C}$$

where  $T$  is the temperature in Celsius.

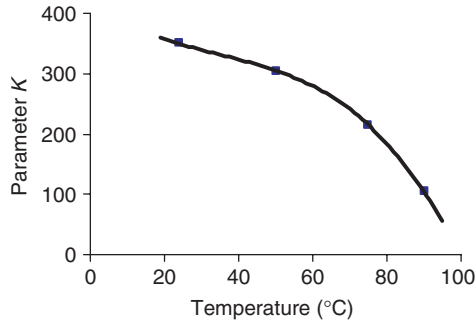


**Figure 23.** Parameter  $K$  of composite A as a function of temperature.

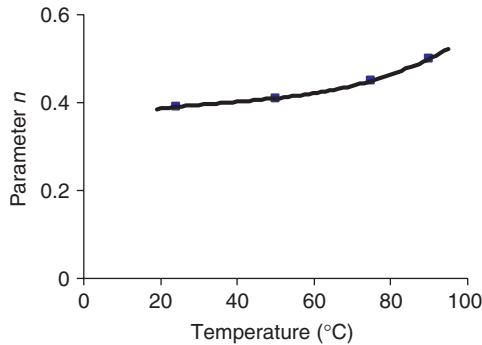


**Figure 24.** Parameter  $n$  of composite A as a function of temperature.

### Damage Parameter

The damage evolution under loading can be monitored by *in situ* stiffness measurements. This is framed in the theory of continuum damage mechanics with the scalar damage parameter  $D$  defined as (Kachanov, 1986):

$$D = 1 - \frac{E}{E_0}$$

where  $E$  is the instantaneous elastic modulus and  $E_0$  is the initial value of the elastic modulus. This damage parameter was determined experimentally (Figures 25 and 26).

### CONCLUSIONS

The mechanical properties of PMMA/ATH composite material are, as expected, functions of temperature and strain rate. At room temperature PMMA/ATH composite can be regarded as a rate insensitive material. At high temperatures, the viscoplasticity properties must be considered for any analysis. The data presented in this article should suffice to obtain all material properties needed for most viscoplastic constitutive model for similar ATH/PMMA particle filled composites. It is also observed that as the strain rate

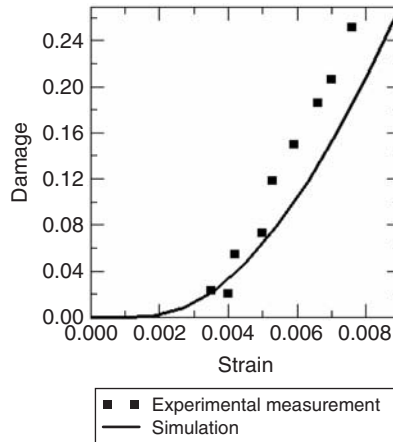


**Figure 25.** Elastic modulus degradation at 24°C.

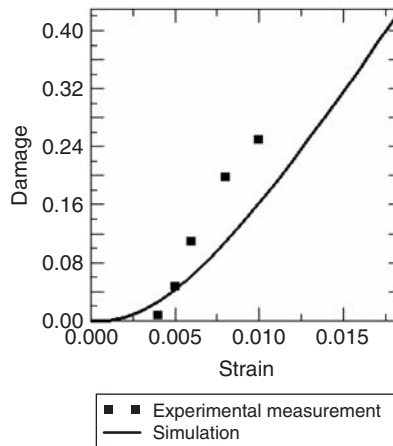


**Figure 26.** Elastic modulus degradation at 75°C.

increases both the Young's modulus and the tensile strength increase, while ductility (plastic deformation at rupture) is independent of strain rate.

An important observation of this study is the fact that creep tests conducted under compressive load yielded the same creep strain rates as the ones conducted under tension, albeit creep strain experienced in compression is much smaller than tension creep tests.

Finite element simulation of the experimental data is the subject of another study. Readers interested in verification of the constitutive model can refer to Nie and Basaran [6] and Basaran and Nie [12].

#### ACKNOWLEDGMENT

Support received from DuPont Surfaces, Yerkes R&D Lab is greatly appreciated.

## REFERENCES

1. Cheng, W.-M., Miller, G.A., Manson, C., Hertzberg, R.W. and Sperling, L.H. (1990). Mechanical Behavior of Poly(methyl methacrylate) Part 1: Tensile Strength and Fracture Toughness, *Journal of Materials Science*, **25**: 1917–1923.
2. Cheng, W.-M., Miller, G.A., Manson, C., Hertzberg, R.W. and Sperling, L.H. (1990). Mechanical Behavior of Poly(methyl methacrylate) Part 2: The Temperature and Frequency Effects on the Fatigue Crack Propagation Behaviour, *Journal of Materials Science*, **25**: 1917–1923.
3. Cheng, W.-M., Miller, G.A., Manson, C., Hertzberg, R.W. and Sperling, L.H. (1990). Mechanical Behavior of Poly(methyl methacrylate). Part 3: Activation Processes for Fracture Mechanism, *Journal of Materials Science*, **25**: 1917–1923.
4. Ferreira, J.M., Costa, J.D. and Capela, C. (1997). Fracture Assessment of PMMA/Si Kitchen Sinks Made from Acrylic Casting Dispersion, *Theoretical and Applied Fracture Mechanics*, **26**: 105–116.
5. Jones, R.M. (1999). *Mechanics of Composite Materials*. **2nd edn**, Taylor & Francis, Philadelphia, PA.
6. Nie, S. and Basaran, C. (2005). A Micromechanical Model for Effective Elastic Properties of Particulate Composites with Imperfect Interfacial Bonds, *Int. J. Solids and Structures*, **42**: 4179–4191.
7. Basaran, C., Nie, S., Hutchins, S. and Ergun, H. (2008). Influence of Interfacial Bond Strength on Fatigue Life and Mechanical Behavior of a Particulate Composite: An Experimental Study, *Int. J. Damage Mechanics*, **17**(2): 123–148.
8. Nie, S., Basaran, C., Hutchins, S. and Ergun, H. (2006). Failure Mechanisms in PMMA/ATH Acrylic Casting Dispersion, *Journal of Mechanical Behavior of Materials*, **17**(2): 79–95.
9. Nielsen, L.E. (1967). Mechanical Properties of Particulate-Filled Systems, *Journal of Composite Materials*, **1**: 100–119.
10. US Patent 3,847,865, Nov 12, 1974, Use of Aluminum Trihydrate in a Poly Methyl Methacrylate Article.
11. Chawla, K.K. (1998). *Composite Materials: Science and Engineering*, **2nd edn**, Springer-Verlag, New York.
12. Basaran, C. and Nie, S. (2007). A Thermodynamic Based Damage Mechanics Model for Particulate Composites, *Int. J. Solids and Structures*, **44**: 1099–1114.
13. Nie, S. (2005). A Micromechanical Study of the Damage Mechanics of Acrylic Particulate Composites Under Thermomechanical Loading, PhD Dissertation Submitted to Dept. of Civil, Structural and Environmental Engineering at the State University of New York at Buffalo.
14. American Society for Testing and Materials, Standard Test for Tensile Properties of Plastics, *Annual Book of ASTM*, Vol. 08.01, ASTM D 638-98 (1999).
15. Ju, J. W. and Chen (1994a). “Micromechanics and Effective Moduli of Elastic Composites Containing Randomly Dispersed Ellipsoidal Inhomogeneities”, *Acta Mechanica*, **103**: 103–121.
16. Kachanov, L.M. (1986). Introduction to Continuum Damage Mechanics, Martinus Nijhoff Dordrecht, The Netherlands.
17. Simo, J.C. and Hughes, T.J.R. (1998). Interdisciplinary Applied Mathematics, Mechanics and Materials, Computational Inelasticity, Springer-Verlag, New York.